A Computational Design of UHS Maraging Stainless Steels Incorporating Composition as well as Austenitisation and Ageing Temperatures as Optimisation Parameters

Wei Xu, P.E. J. Rivera-Diaz-Del-Castillo, Sybrand van Der Zwaag

A Computational Design of UHS Maraging Stainless Steels Incorporating Composition as well as Austenitisation and Ageing Temperatures as Optimisation Parameters

Journal:	*Philosophical Magazine & Philosophical Magazine Letters*
Manuscript ID:	TPHM-09-Feb-0083.R1
Journal Selection:	Philosophical Magazine
Date Submitted by the Author:	21-Apr-2009
Complete List of Authors:	Xu, Wei; Materials Innovation Institute M2i; Delft University of Technology, Fundamentals of Advanced Materials Group, Faculty of Aerospace Engineering Rivera-Diaz-del-Castillo, P.E. J.; Delft University of Technology, Fundamentals of Advanced Materials Group, Faculty of Aerospace Engineering van der Zwaag, Sybrand; Delft University of Technology, Fundamentals of Advanced Materials Group, Faculty of Aerospace Engineering
Keywords:	age-hardening, carbides, precipitation, stainless steels, thermodynamics
Keywords (user supplied):	genetic algorithm, alloy design

A Computational Design of UHS Maraging Stainless Steels Incorporating Composition as well as Austenitisation and Ageing Temperatures as Optimisation Parameters

W. Xu[a,b], P.E. J. Rivera-Díaz-del-Castillo[b], S. van der Zwaag[b]

[a] *Materials Innovation Institute M2i, Kluyverweg 1, 2629 HS, Delft, The Netherlands;*

[b] *Fundamentals of Advanced Materials Group, Faculty of Aerospace Engineering, Delft University of Technology, Kluyverweg 1, 2629 HS, Delft, the Netherlands.*

W. Xu:

Email: w.xu@tudelft.nl.

Tel: 0031 15 278 5218 Fax: 003115278 4472

P.E. J. Rivera-Díaz-del-Castillo

Email: P.E.J.Rivera@tudelft.nl

Tel: 0031 15 278 84559 Fax: 003115278 4472

S. van der Zwaag

Email: S.vanderZwaag@tudelft.nl

Tel: 0031 15 278 82248 Fax: 003115278 4472

Abstract

An extended integral alloy design approach for the development of new ultra high strength maraging steels is presented which incorporates not only chemical composition effects but also criteria accounting for the influence of the entire heat treatment. The approach accounts for the desired strengthening precipitates formed during the final ageing treatment as well as undesirable equilibrium phases present during the preceding high temperature homogenisation treatment. The results are compared with the predictions of a previous model which accounted for the combination of composition and the final precipitation tempering stage only.

Keyword: maraging steels; composition, precipitation; carbide, δ-ferrite, thermodynamics, genetic algorithm, alloy design.

1. Introduction

The microstructure of ultra-high strength (UHS) stainless steels is of great complexity and results from various heat treatment steps aimed at the control of different aspects of the desired final microstructure. In the case of maraging steels, the microstructure consists of a martensite matrix typically containing various species of strengthening precipitates. This microstructure is obtained via a two step heat treatment: solutionising to achieve a homogenous austenite state followed by quench to room temperature to generate the martensitic matrix structure and further ageing at a modest temperature to allow precipitation in this finely grained matrix structure. .

Over the last decades, computational thermodynamics supplementing and replacing the experimental approach [1-4] has become a more efficient and powerful tool in providing guidance for alloy design [5, 6] and process development [7-9]. Some approaches, such as artificial neural networks (ANN), may be an aid in guiding both [10, 11]. However, these are statistically rooted, and cannot supply compositions and/or processing parameters outside the data ranges employed to train the network. In order to overcome this limitation, recently, a thermokinetics based computational alloy design model has been presented by Xu et al. [12-14] in which the alloy composition and ageing temperature are designed and optimised simultaneously in an integral manner. That model also provided a thermodynamic justification for the optimal ageing temperatures reported for various existing maraging steels. The model was focused on the phases formed during ageing and ignored those phases that may form during the prior casting and homogenisation steps.

Undesirable phases left over from the high temperature casting and homogenisation steps include primary carbides (MC/M_2C), δ-ferrite and retained austenite. The primary carbides form during solidification both intergranularly and intragranularly, and they display a low number density per unit volume and a large size [15, 16]. They frequently act as crack initiators and may also cause intergranular corrosion, although some intergranular carbides may display a positive pinning effect on limiting the growth of prior austenite grains during austenitisation/solution treatment. However, some controversy still exists concerning the role of prior austenite grain size played on final mechanical properties [1, 17]. For some conditions, all or part of the primary carbides can be dissolved during the austenitisation/solution heat treatment, and subsequently reprecipitate as a fine secondary strengthening phase during the ageing treatment, or when these materials are subjected to high-temperature applications [15]. Moreover, δ-ferrite normally appears in the as cast condition and its volume fraction decreases during austenitisation and solution treatment [18]. The presence of δ-ferrite in maraging steels can lead to inferior mechanical and corrosion resistant properties [19]. More importantly, the content of δ-ferrite also influences the distribution of alloying elements and therefore affects the martensitic transformation present upon quenching, as well as the subsequent precipitation process during ageing [18]. The retained austenite in the pre-ageing condition may increase the ductility while decrease the strength. However, austenite which transforms into martensite upon quenching and its retained form are thermodynamically identical, and therefore cannot be tackled employing our computational framework without invoking kinetic criteria.

In the present work, our previous genetic algorithm based thermokinetic model for precipitation hardened maraging stainless steels design is further developed incorporating new criteria to avoid the presence of undesirable phases at the homogenisation stage. The alloy composition, together with ageing and austenitisation/solution treatment temperatures are optimised simultaneously in an integrated manner. The alloys utilising different strengthening precipitates are designed and results are compared to our previous calculations and existing commercial alloys.

2. Model

The alloys are designed through a computational approach coupling a genetic algorithm with optimisation criteria based on thermodynamic, kinetic and mechanical principles. The model focuses on the martensite formation and precipitation strengthening contribution resulting from solutionising and ageing treatment. Hot/cold rolling, dynamic recovery and recrystallization effects are not taken into account. The microstructures considered and the resulting alloy design approach are summarized below. A fully detailed description of the original method, not covering the new austenitisation criteria presented in this work, can be found elsewhere [12-14].

The desired combination of ultra high strength (UHS) and good toughness can be realised via uniformly dispersed fine precipitates of desirable species in a lath martensite matrix. Corrosion resistance property can be obtained by the formation of a Cr-rich oxide film on the material surface.

2.1 Martensite Formation

To ensure full lath martensitic structures after quenching, experimental observations on regular engineering steels have shown that an Ms temperature above 423 K is required [5]. For each alloy computationally considered, the Ms temperature is estimated as the first step using the model proposed by Ishida [20] and enforced as a go/nogo criterion of Ms ≥ 473K, as illustrated in Figure 1.

$$Ms(\mathrm{K}) = 818 - 33000\times C_c + 200\times C_{Al} + 700\times C_{Co} - 1400\times C_{Cr} - 1300\times C_{Cu} \\ -2300\times C_{Mn} - 500\times C_{Mo} - 400\times C_{Nb} - 1300\times C_{Ni} - 700\times C_{Si} + 300\times C_{Ti} + 400\times C_V, \quad (1)$$

where all the concentrations are given in weight fraction.

It is worth noting that more sophisticated approaches such as Ghosh-Olson model [21, 22] may lead to more accurate predictions of Ms temperature, but at a greater computational cost. Eq.1 is employed as a first approximation for reducing computational time. Our previous work justifies the use of this formula in designing ultra high strength stainless steels [12].

2.2 Ageing Treatment: Precipitation in a Cr-rich Matrix

Ageing is a key treatment for maraging steels because it determines the type of precipitates and populations to be formed in the lath martensite matrix. It is well documented that the formation of MC carbides [15], Cu particles [23] and NiAl/Ni_3Ti intermetallic precipitates [24] have a paramount contribution to the strength. It is also preferred to have the precipitates dispersed in a dense and homogeneous manner so as to achieve the best strengthening effect. Therefore, by assuming a mixture of sheared

and by-passed precipitate strengthening mechanisms to be presented [14], the precipitation strengthening contribution is estimated as:

$$\sigma_p \propto f_v^{1/2} r^{-1/2} \quad \text{(Eq. 2)}$$

where f_v is the equilibrium volume fraction of the precipitate at the ageing temperature (T_{Age}) and r is the critical precipitate nuclei size, which is inversely proportional to the thermodynamic driving force for precipitation. The use of this estimation was justified in our previous work [14], where several precipitation hardened maraging steels show the relationship (Eq.2) is approximately followed employing a single constant. For the compositions fulfilling the Ms temperature criterion, the thermodynamic equilibrium is calculated at the ageing temperature and relevant information is recorded for further evaluation. The Cr concentration in the matrix upon completion of precipitation is artificially imposed at $C_{Cr}^{Matrix} \geq 12$ wt% in order to ensure the formation of a Cr-rich corrosion resistant film. The amounts of undesirable phases are summed up and the maximum allowed volume fraction of all those phases together is arbitrarily set at 1%. Only solutions (composition and temperatures) fulfilling these criteria are taken as a valid candidate for the next appraisal: the equilibrium phases present during the austenitisation step prior to the martensitic quench.

2.3 Austenitisation/Solution Treatment

The austenitisation/solution treatment is of great importance in order to achieve the desirable microstructure. The austenitisation and the solution treatment are two separate processes, however, they are given the same relevance in the calculation in terms of avoiding undesirable phases in the pre-ageing condition. Thermodynamic equilibrium is therefore calculated at only one pre-aging temperature, denoted as T_{Aus}. In order to obtain a near pure austenite matrix with a similar composition to the alloy

so that full transformation into lath martensite during quenching takes place as the Ms criterion is followed, a new go/nogo condition is enforced by requiring an austenite volume fraction above 99% in equilibrium at T_{Aus}. Due to the positive pining effects of primary carbides, a small amount of primary carbides is allowed at a maximum level of 0.5 % in volume.

The entire solution evaluation algorithm is shown in Figure 1. The precipitation strengthening contribution estimated by Eq.2 is only calculated for those alloy candidates (composition and temperatures) which fulfil all criteria mentioned above. The calculations are embedded in a genetic optimisation algorithm in order to maximize the search speed over a large search space.

3. Model application

Steel compositions containing up to 13 alloying elements were considered: C, Cr, Ni, Ti, Mo, Al, Cu, Co, Nb, N, V, Mn and Si. The concentrations were varied within compositional ranges (Table 1) based on industrial and technological constraints related to cost price and ability to fabricate the alloys. Each component was allowed to take 32 potential concentration levels equally distributed over its compositional range. The ageing temperature and austenitisation/solution treatment temperature were allowed to vary within the range of 698-853 K and 1223-1533 K with intervals of 5 and 10 K respectively.

Three alloy design scenarios involving different strengthening precipitate systems were explored: 1) MC carbides, 2) Cu particles and 3) Ni-rich intermetallics (NiAl

and Ni_3Ti). The alloys resulting from these systems will be hereon termed alloy 1, 2 and 3, respectively. Two series of alloys were computationally designed: C series (1C, 2C and 3C) with fixed T_{Age} of 773 K and T_{Aus} of 1473 K, and D series (1D, 2D and 3D) in which T_{Age} and T_{Aus} are allowed to vary in the ranges mentioned above. The alloy compositions, T_{Age} and T_{Aus} are summarised in Table 2. For comparison purpose, the compositions found by a previous model [12] not taking into account the austenitisation/solution treatment effects are also listed in Table 2. They are, named alloys 1A-3A (for a fixed ageing temperature of 773K) and alloys 1B-3B (for a variable ageing temperature), respectively.

From Table 2 it can be observed that the concentrations of C and Ti in alloys 1C and 1D have decreased significantly with respect to those for alloys 1A and 1B. This is because the high C and Ti contents in alloys 1A and 1B lead to the formation of a considerable amount of primary carbides as experimentally observed [25]. Moreover, the concentrations of V and Nb are higher in alloy 1D than in 1C by allowing the austenitisation temperature increase from 1473 K to 1553 K. The V concentration is even higher than alloys 1A and 1B. This is due to V has a higher solubility in austenite. Furthermore, because of the partial substitution of Ti by V, the formability of second phase MC carbide during ageing remains maximized while avoiding the primary carbides during austenitisation. However, the amount of carbide strengthening precipitates is expected to decrease due to the lower C concentration. Ni, Co and Si also adjust their concentrations to follow other go/nogo criteria.

In alloys 2C and 2D, the concentration of Cr decreases slightly and Ni increases. This is expected as Ni is a strong austenite stabilizer and Cr is a ferrite stabilizer. The

concentration of Ti increases while V decreases; Cu decreases but Co increases. This is all because of the solubility of alloying elements in austenite and their effects on the formation of other undesirable phases such as δ-ferrite and primary carbides. The new criteria based on austenitisation seems to have insignificant effects on alloys 3C and 3D because the high Ni and Al concentrations leading to NiAl/Ni_3Ti precipitation can be well dissolved in austenite. For all alloys 1-3, the optimal austenitisation temperatures in D series tend to be close to the upper limit in order to increase the solubility of alloying elements while avoiding the formation of δ-ferrite. The best ageing temperature to stimulate the formation of desirable strengthening precipitates is lower than the fixed value of 773 K, but the new temperature still falls within the range of the experimental optima [12].

4. Discussion

In order to illustrate the effect of the new austenitisation criteria on the precipitation strengthening capability, the overall strengthening contribution for the three systems and the four optimisation strategies explored are compared in Figure 2. The precipitation strengthening factor of alloy 1 is drastically decreased for alloys 1C and 1D because of the lower C required for avoiding primary carbides during austenitisation. In alloys 2C and 3C, the strengthening contributions of Cu and NiAl/Ni_3Ti precipitates also drop notably, while through increasing austenitisation temperature and decreasing ageing temperature, they can be well compensated and become comparable to those in the A and B series. The volume fractions, precipitation driving forces and normalized precipitation strengthening contributions of each precipitate in alloys 1D-3D are plotted in Figure 3(a)-(c) respectively. For

validation purposes, in Figure 3 the model was also applied to 11 commercial precipitate strengthening steels which are grouped according to their main strengthening systems. Although the precipitation strengthening factors are lower than those displayed by the A and B series (figure 2), the new alloys 1D-3D still show improved strength over their existing counterparts. It is also important to point out that all new alloys 1D-3D possess multiple strengthening precipitate systems despite the fact that they were designed to be strengthened by one kind of precipitate only. The existence of the additional desirable precipitate species will further contribute to the strength.

To demonstrate the effects of all criteria on alloy composition optimisation, alloy 1A was taken as the baseline to explore the binary compositional effects of C-Ti and C-Cr, (keeping the levels of all other elements as found by the optimisation scheme) as shown in Figure 4 and Figure 5 respectively. For this purpose, the composition domains studied have been extended beyond the original search ranges in Table 1, marked by the two orthogonal solid lines in the bottom or top left hand corner. The colour contour of the background in these figures indicates the degree of strengthening contribution obtained due to precipitation at 773 K. The black vertical patterns in Figures 4(a) and 5(a) superimposed on the colour coded background display the (forbidden) composition domains where Ms temperature is below 473 K; the horizontal black patterns mask the (forbidden) area in which the total amount of undesirable phases is over 1% in volume and the forward slash region shows the (forbidden) domain where Cr concentration is below 12 wt% after the completion of precipitation. The scatted black spots show compositions where ThermoCalc equilibrium calculations were not successfully performed. The unhashed areas in

Figures 4(a) and 5(a) unveil the composition domains in which precipitation strengthening factor is maximized, while meeting the constraints mentioned above. The solid stars show the concentration value of alloy 1A, which is located exactly at the maximum strengthening level in the uncovered area of the searching domain. Imposing the new criteria of austenitisation treatment as discussed previously, the compositional domain where austenite volume fraction is less than 99% at 1473 K is masked by white horizontal lines and the area where the primary carbides volume fraction at 1473 K exceeds 0.005 is indicated by the vertical white line pattern. It can be seen in both Figures 4(b) and 5(b) that, the new criteria imposed covers all of the search area. If all criteria are applied simultaneously, Figures 4(c) and 5(c) show that there are no solutions for C, Ti and Cr concentrations, given the concentrations of the remaining elements stay the same as in alloy 1A. Therefore, the new optimal composition considering austenitisation treatment has to be found somewhere else in the entire search domain.

The same type of plot is generated based on alloy 1D, which was optimised for the carbide system considering the entire heat treatment. The components and temperatures are paired as C-Ti, C-Cr, C-T_{Age} and C-T_{Aus}. The results are shown in Figures 6-9, respectively. In Figure 6(a), a large open area can be observed while most of it (the high C and high Ti region) is covered in Figure 6(b) because the formation of primary TiC carbide violates the criteria of austenite fraction and primary carbides itself. However, there is still a solution area meeting all criteria (Figure 6(c)) in which the black star shows the location of highest strength level which is exactly the composition of C and Ti of alloy 1D. Figure 7 shows the same trend that high carbon concentration tends to promote the formation of primary

carbides as demonstrated by the vertical white lines in Figure 7(b) and high Cr content leads to formation of non-austenite phase due to the limited solubility of Cr in austenite as indicated by the horizontal white lines. There is a very small area which fulfils all conditions in the searching space and the solution is indicated by the star in Figure 7(c). The background colour in Figure 8(a) shows that there is a preferred ageing temperature range around 740 K depending on the carbon concentration. Again, Figure 8(b) shows the high carbon concentration results in primary carbides promotion and very low carbon leads to the formation of other phases, for instance, δ-ferrite. The strengthening level in Figure 9 only changes with carbon content because it is calculated for the ageing temperature of 743 K and is not directly related to the austenitisation temperature. Looking at the upper edge of the vertical white pattern in Figure 9(b), it shows that a higher austenitisation temperature is required for higher carbon content in order to dissolve all carbon in the austenite without forming primary carbides. However, if the austenitisation temperature is too high, liquid may start to be present as shown by the white backslash in Figure 9(b). When all criteria are taken into account, the best C concentration and austenitisation temperature are found to be 0.08 wt% and 1533 K, respectively.

In order to visualize compositional and temperature effects on the strengthening factor, as well as on all other criteria in more detail, a simulation was performed in which the composition and temperature are varied taking alloy 1D as a reference. In Figure 10, the vertical axis is the normalized concentration or temperature where 1 stands for the minimum and 32 represents the maximum of the searching range. In each group, the first colour bar (STR) represents the strengthening contribution, calculated by fixing all the remaining composition and temperature parameter values as of alloy 1D. The

second bar (TMS) stands for the Ms temperature criterion of which the white part is the window fulfilling Ms $\geq$ 473 K and the gray scaled part indicates the unfavourableness regarding this criterion (the darker the worse). Following the same principle, the other bars referred to go/nogo criteria of total volume amount of undesirable phases during ageing (VF), Cr concentration in the matrix (Cr), austenite percentage in austenitisation treatment (Aus) and the amount of primary carbides (Car) are plotted next to each other. The best solution should be found with the highest strengthening factor in the first column, while all the go/nogo criteria are fulfilled (represented by white colour instead of gray scale). The black circles demonstrate such values in each group and all of them are found to be the same as in alloy 1D, which provides strong evidence that the alloy design and optimisation approach described above is applicable for such complex system accounting for the entire heat treatment. The results also show that there are very narrow solution windows for C, Cr, Ni, Ti, Mo, Al and T_{Aus} while for the rest of the parameters, the windows are relatively big. For Nb, there is no unfulfilled criterion in the considered searching range. Focusing on strengthening precipitation, the STR bars show that C, Ni, Ti, Nb and T_{Age} have the strongest strengthening effects. On the hand, for go/nogo criteria, the most important parameters are: (1) C, Cr, Ni, Mo and Cu for Ms temperature criterion (TMS). (2) C, Cr, Ni, Ti, Mo, V and T_{Age} for the total amount of undesirable phases (VF). (3) Ni and Ti for the Cr concentration in the matrix (Cr). (4) Cr, Ni, Ti, Mo, Al, Cu and T_{Aus} for the austenite fraction (Aus). (5) C, Cr, Ti, Mo, Al, Cu, Si and T_{Aus} for the primary carbides (Car). Given the alloy 1D as the baseline, the criteria of TMS, VF, Aus and Car blocked most of the windows and are therefore the most difficult ones to be fulfilled, but this statement may not hold true for other systems.

5. Conclusions

A thermokinetics based computational alloy design model accounting for chemical composition as well as the phases present during the entire heat treatment is applied to conceive novel UHS maraging stainless steels. The alloys are strengthened by promoting the formation of various families of precipitate systems while avoiding the appearance of undesirable microstructures during critical stages of the heat treatment. The alloy compositions, as well as the austenitisation/solution and ageing temperatures are optimised simultaneously in an integrated manner. Compared to a previous design model including only the aging stage, the consideration of undesirable phases present during the austenitisation treatment leads to significant compositional changes in the alloys strengthened by MC carbides and Cu particles, but minor changes in the system utilizing NiAl/Ni_3Ti. Although the precipitate strengthening contributions decrease to different extent due to the new austenitisation criteria applied, the newly designed alloys are predicted to reach strength levels beyond those of existing commercial counterparts.

Acknowledgment

This research was carried out under the project number MC5.04192 in the framework of the Research Program of the Materials innovation institute M2i (www.m2i.nl), the former Netherlands Institute for Metals Research.

References

[1] Y. He, K. Yang, W. S. Qu, F. Y. Kong, G. Y. Su, Materials Science and Technology 19 (2003) 117-124.

[2] Y. He, K. Yang, W. Sha, Metallurgical and Materials Transactions A: Physical Metallurgy and Materials Science 36 (2005) 2273-2287.

[3] P. Michaud, D. Delagnes, P. Lamesle, M. H. Mathon, C. Levaillant, Acta Materialia 55 (2007) 4877-4889.

[4] P. Würzinger, R. Rabitsch, W. Meyer, Journal of Materials Science 39 (2004) 7295-7302.

[5] C. E. Campbell, G. B. Olson, Journal of Computer-Aided Materials Design 7 (2000) 145-170.

[6] V. Trabadelo, S. Giménez, T. Gómez-Acebo, I. Iturriza, Scripta Materialia 53 (2005) 287-292.

[7] J. Agren, Materials Science Forum 163-6 (1994) 3-14.

[8] U. E. Klotz, C. Solenthaler, P. J. Uggowitzer, Materials Science and Engineering A 476 (2008) 186-194.

[9] B. J. Lee, H. D. Kim, J. H. Hong, Metallurgical and Materials Transactions A: Physical Metallurgy and Materials Science 29 (1998) 1441-1447.

[10] H. K. D. H. Bhadeshia, ISIJ International 39 (1999) 966-979.

[11] Z. Guo, W. Sha, Computational Materials Science 29 (2004) 12-28.

[12] W. Xu, P. E. J. Rivera-Diaz-del-Castillo, S. van der Zwaag, Computational Materials Science. 45 (2009) 467-473.

[13] W. Xu, P. E. J. Rivera-Díaz-del-Castillo, S. van der Zwaag, Computational Materials Science. 44 (2008) 678-689.

[14] W. Xu, P. E. J. Rivera-Díaz-del-Castillo, S. van der Zwaag, Philosophical Magazine. 88 (2008) 1825-1833.

[15] A. F. Padilha, P. R. Rios, ISIJ International 42 (2002) 325-337.

[16] A. F. Padilha, G. Schanz, K. Anderko, Journal of Nuclear Materials 105 (1982) 77-92.

[17] H. J. Rack, Materials Science and Engineering 34 (1978) 263-270.

[18] D. T. Llewellyn, R. C. Hudd, Steels: Metallurgy and Applications, Butterworth-Heinemann, Oxford, 1998.

[19] H. Shaikh, H. S. Khatak, S. K. Seshadri, J. B. Gnanamoorthy, P. Rodriguez, Metallurgical and Materials Transactions A 26 (1995) 1859-1868.

[20] K. Ishida, Journal of Alloys and Compounds 220 (1995) 126-131.

[21] G. Ghosh, G. B. Olson, Acta Metallurgica et Materialia 42 (1994) 3361-3370.

[22] G. Ghosh, G. B. Olson, Acta Metallurgica et Materialia 42 (1994) 3371-3379.

[23] H. R. H. Bajguirani, C. Servant, G. Cizeron, Acta Metallurgica et Materialia 41 (1993) 1613-1623.

[24] K. Stiller, M. Hättestrand, F. Danoix, Acta Materialia 46 (1998) 6063-6073.

[25] W. Xu, P. E. J. Rivera-Díaz-del-Castillo, S. van der Zwaag, in: TMS 2009 Annual Meeting and Exhibition: Synergies of Computational and Experimental Materials Science, San Francisco, 2009.

Table 1 Concentration ranges of all components employed in the optimisation (in weight percentage).

	C	Cr	Ni	Ti	Mo	Al	Cu	Co	Nb	N	V	Mn	Si	Fe
Min	0.05	12.00	1.00	0.01	0.50	0.01	0.50	0.01	0.01	0.01	0.01	0.50	0.30	Bal.
Max	0.20	20.00	15.00	1.50	10.00	1.00	10.00	2.00	0.10	0.01	0.20	0.50	1.00	

Table 2 Compositions and heat treatment temperatures of designed alloy systems 1 (Carbide based), 2 (Cu based) and 3 (Ni_3Ti/NiAl based), considering only ageing treatment at fixed temperature of T_{Age}=773 K (A series) and varying T_{Age} (B series); considering both ageing and austenitisation/solution treatment at fixed T_{Age}=773 K and T_{Aus}=1473 K (C series) and varying T_{Age} and T_{Aus} (D series). Concentrations are in weight percent.

	C	Cr	Ni	Ti	Mo	Al	Cu	Co	Nb	N	V	Mn	Si	T_{Age}	T_{Aus}
1A	0.20	12.00	2.81	1.50	0.50	0.01	5.10	2.00	0.10	0.01	0.01	0.50	1.00	773	--
1B	0.20	12.00	2.81	1.50	0.50	0.01	5.10	2.00	0.10	0.01	0.01	0.50	1.00	738	--
1C	0.08	12.00	3.26	0.39	0.50	0.01	0.50	1.04	0.05	0.01	0.03	0.50	0.32	773	1473
1D	0.08	12.00	4.61	0.35	0.50	0.01	5.10	0.27	0.10	0.01	0.20	0.50	0.64	743	1533

	C	Cr	Ni	Ti	Mo	Al	Cu	Co	Nb	N	V	Mn	Si	T_{Age}	T_{Aus}
2A	0.05	12.26	1.00	0.01	0.50	0.01	10.00	1.04	0.10	0.01	0.13	0.50	1.00	773	--
2B	0.05	12.26	1.00	0.01	0.50	0.01	10.00	1.04	0.10	0.01	0.10	0.50	1.00	738	--
2C	0.05	12.00	3.26	0.44	0.50	0.01	8.16	1.61	0.10	0.01	0.03	0.50	0.64	773	1473
2D	0.05	12.00	2.81	0.20	0.50	0.01	8.77	1.55	0.10	0.01	0.03	0.50	1.00	718	1523

	C	Cr	Ni	Ti	Mo	Al	Cu	Co	Nb	N	V	Mn	Si	T_{Age}	T_{Aus}
3A	0.05	12.26	11.39	1.50	0.81	1.00	0.50	2.00	0.07	0.01	0.18	0.50	1.00	773	--
3B	0.05	12.00	11.39	1.50	1.11	1.00	0.50	2.00	0.01	0.01	0.10	0.50	1.00	733	--
3C	0.05	12.00	11.39	0.73	0.81	1.00	0.50	2.00	0.05	0.01	0.01	0.50	0.91	773	1473
3D	0.05	12.00	11.39	1.12	0.81	1.00	0.50	2.00	0.01	0.01	0.20	0.50	0.95	728	1533

Figure 1 Algorithm of the thermodynamic calculation and criteria evaluation.

Figure 2 Comparison of normalized precipitation strengthening contributions of alloys 1-3, A-D series.

Figure 3 Comparison of designed (1D-3D) and existing grades: (a) volume fraction of precipitates, (b) driving force for precipitation and (c) normalized precipitation strengthening factor calculated by Eq. 2. The symbols indicate values for commercial steels.

Figure 4 Binary compositional effects of C-Ti based on alloy 1A. The background contour shows the carbide precipitation strengthening factor as scaled in (c). The black vertical, horizontal and forward slash patterns demonstrate the area not fulfilling the go/nogo criteria of Ms temperature, total amount of undesirable phases and Cr concentration in the matrix, respectively (a). The white horizontal and vertical patterns indicate the new criteria for volume fractions of austenite and primary carbides initiating from austenitisation/solution treatment (b). The combination of both sets of criteria is shown in (c). The scatted black spots show compositions where ThermoCalc equilibrium calculation can not be successfully performed. The composition with a star indicates the optimal (alloy 1A) solution. All concentrations are given in weight fraction.

Figure 5 Binary compositional effects of C-Cr based on alloy 1A. The patterns are the same as described in the caption of Figure 4.

Figure 6 Binary compositional effects of C-Ti based on alloy 1D. The patterns are the same as described in the caption of Figure 4.

Figure 7 Binary compositional effects of C-Cr based on alloy 1D. The patterns are the same as described in the caption of Figure 4.

Figure 8 Binary effects of C-T_{Age} based on alloy 1D. The patterns are the same as described in the caption of Figure 4.

Figure 9 Binary effects of C-T_{Aus} based on alloy 1D. The patterns are the same as described in the caption of Figure 4.

Figure 10 The effects of alloy composition and austenitisation/ageing temperatures on strengthening factor and all go/nogo criteria: precipitation strengthening factor (STR), Ms temperature (TMS), volume fraction of all desirable phases during ageing (VF), Cr concentration in the matrix (Cr), austenite volume fraction in the austenitisation treatment (Aus) and the volume fraction of primary carbides (Car). Red and white represent the desired values in the coloured and gray scales. Alloy 1D is taken as the base line for the analysis.

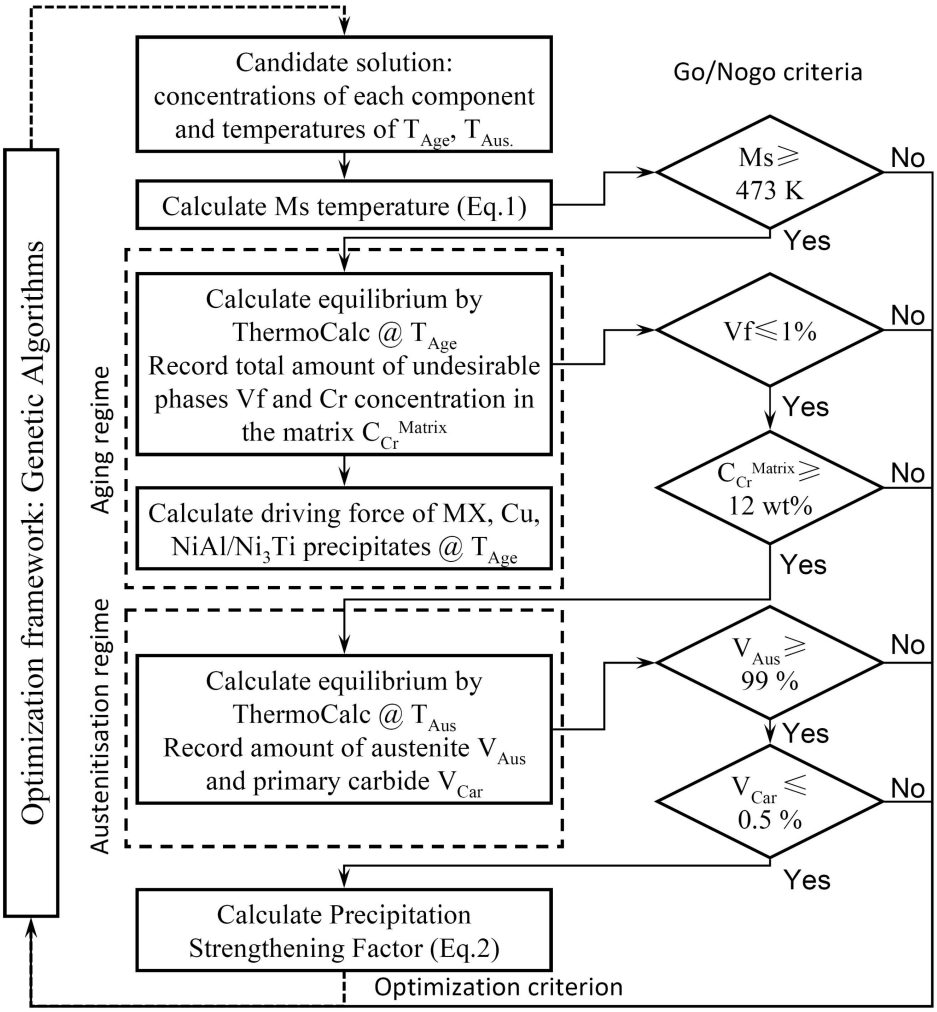

119x125mm (600 x 600 DPI)

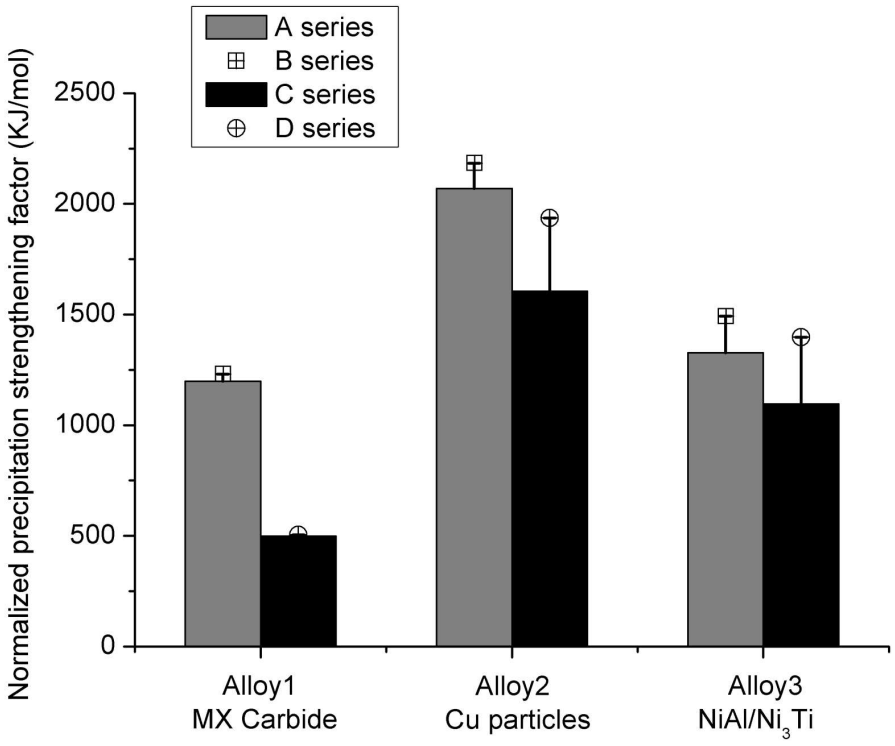

148x126mm (300 x 300 DPI)

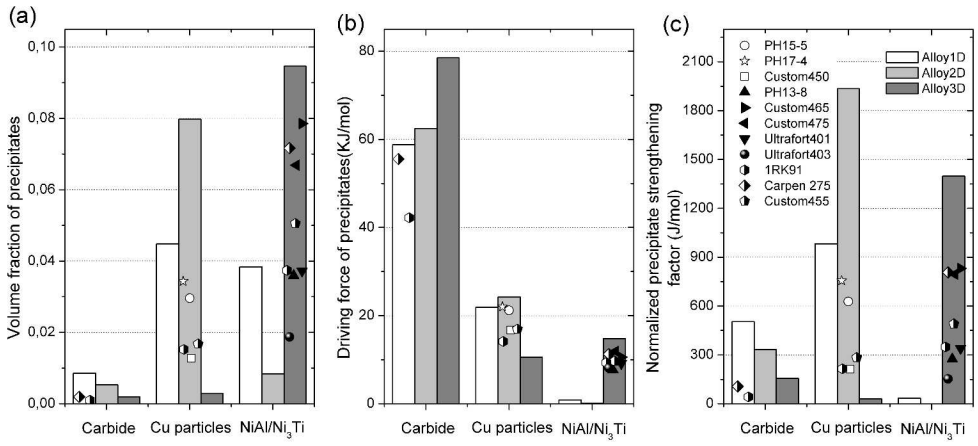

198x91mm (600 x 600 DPI)

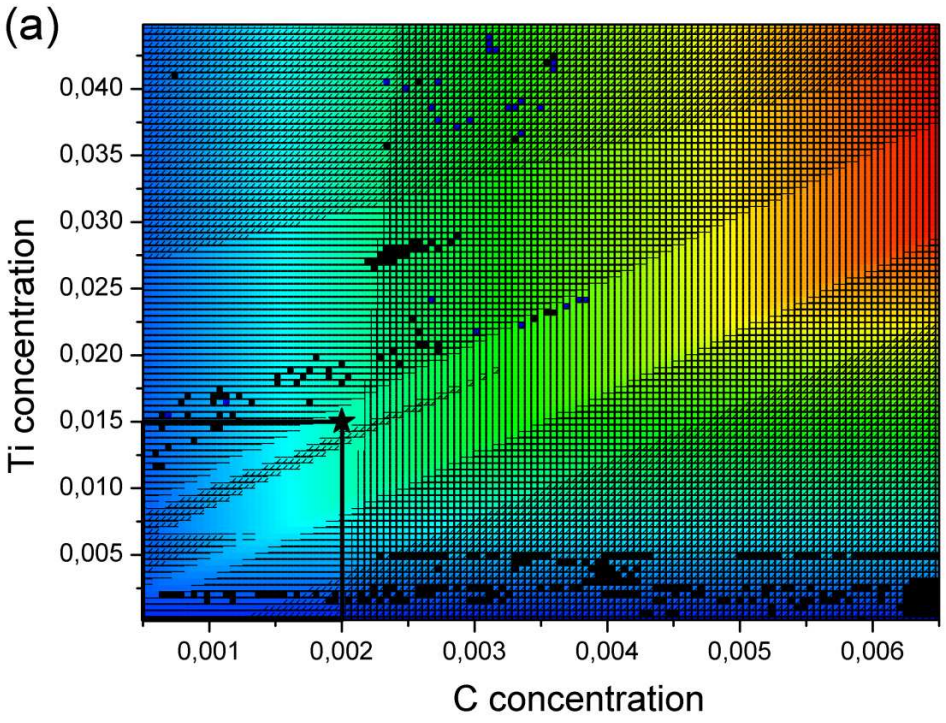

99x74mm (300 x 300 DPI)

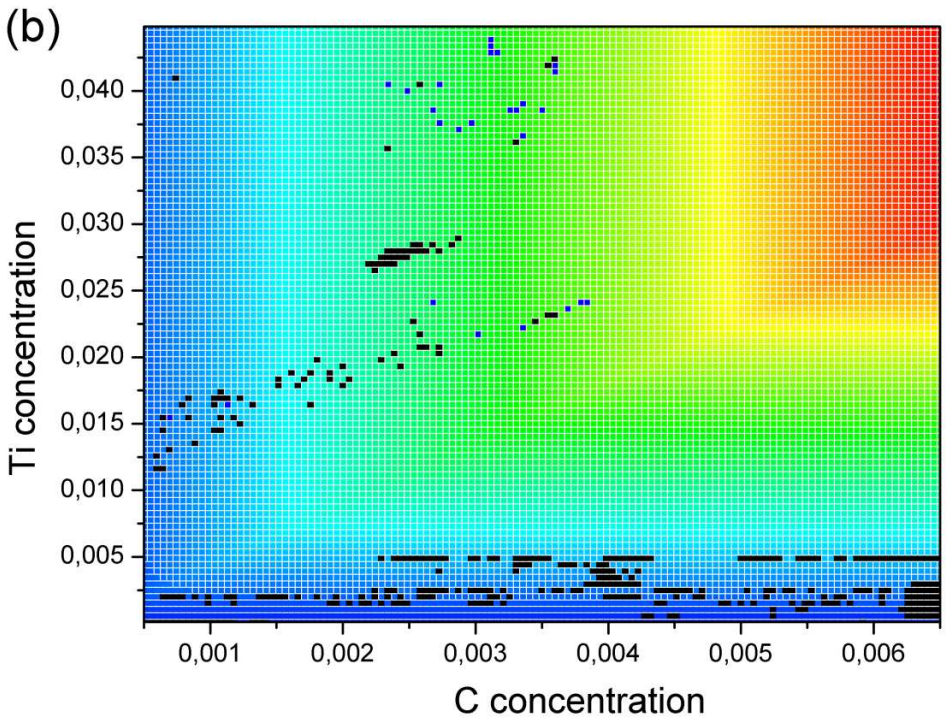

99x74mm (300 x 300 DPI)

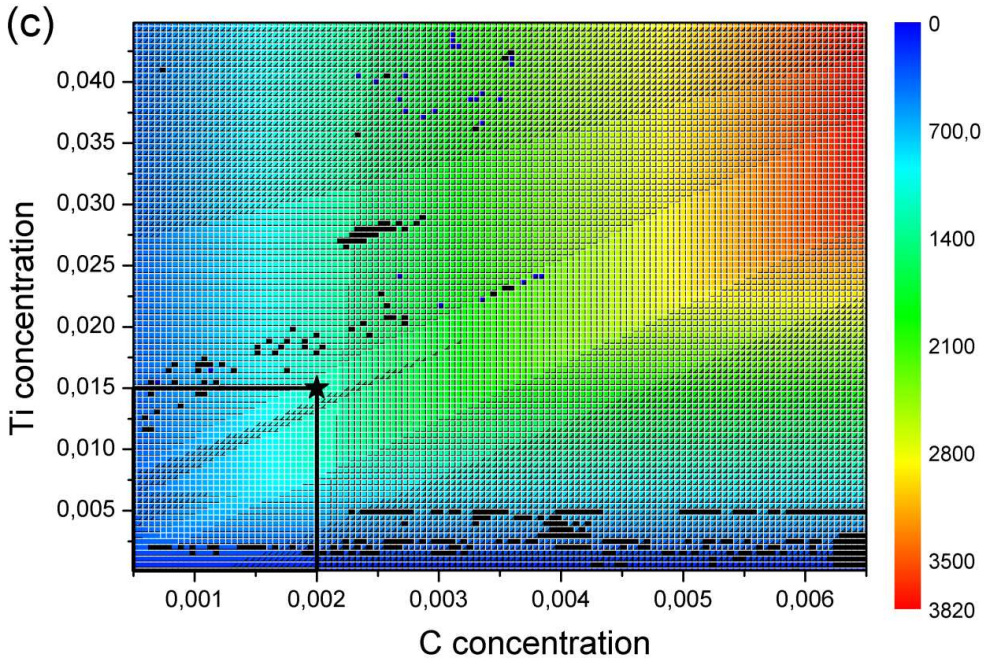

107x74mm (300 x 300 DPI)

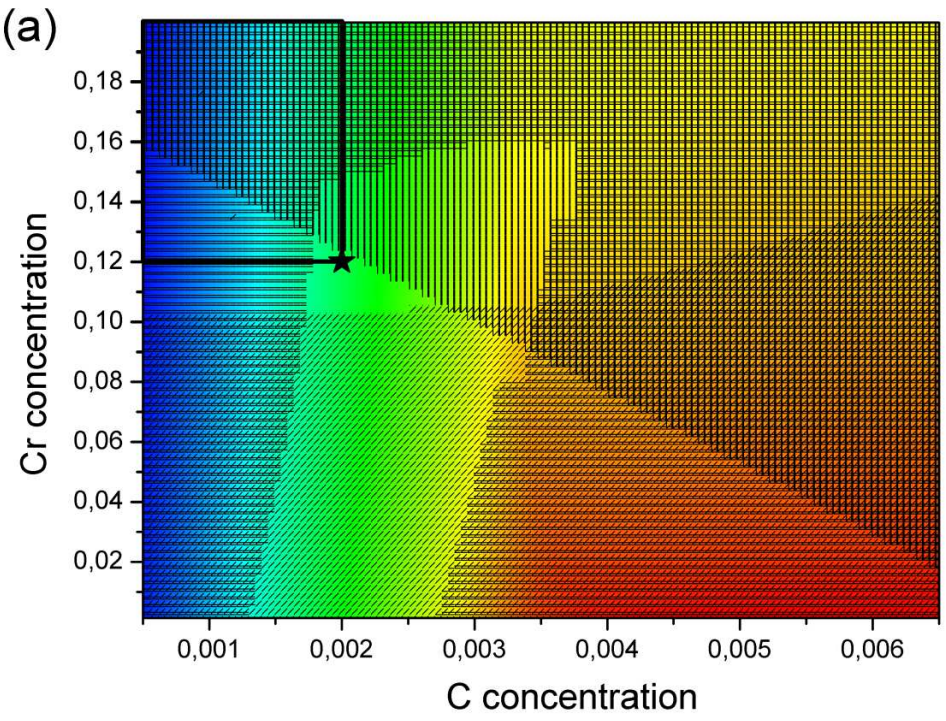

99x74mm (300 x 300 DPI)

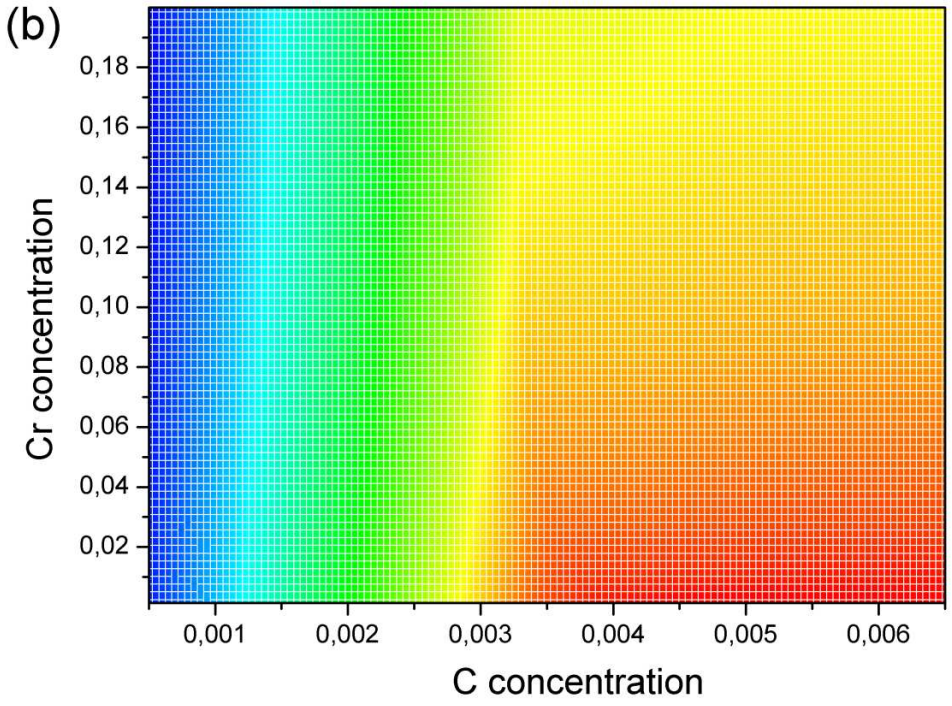

99x74mm (300 x 300 DPI)

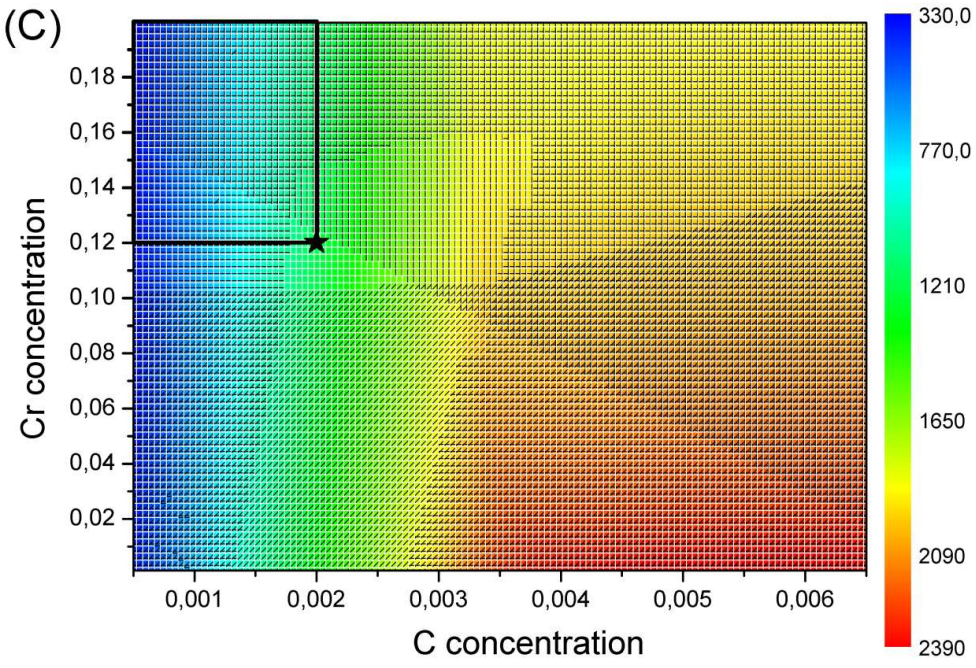

107x74mm (300 x 300 DPI)

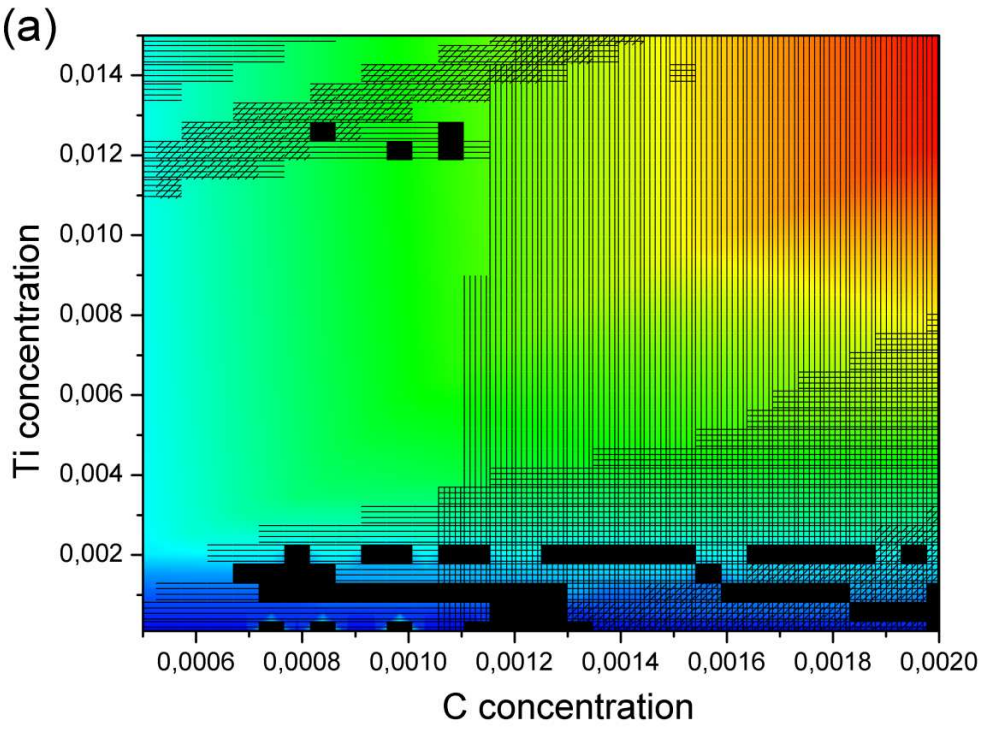

99x74mm (300 x 300 DPI)

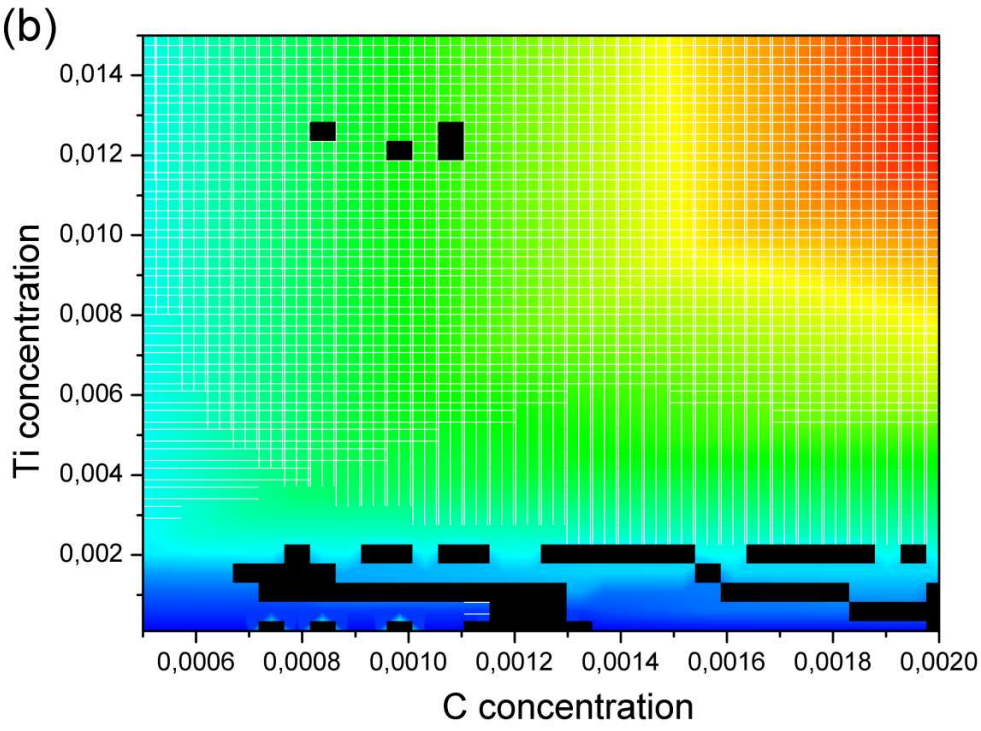

99x74mm (300 x 300 DPI)

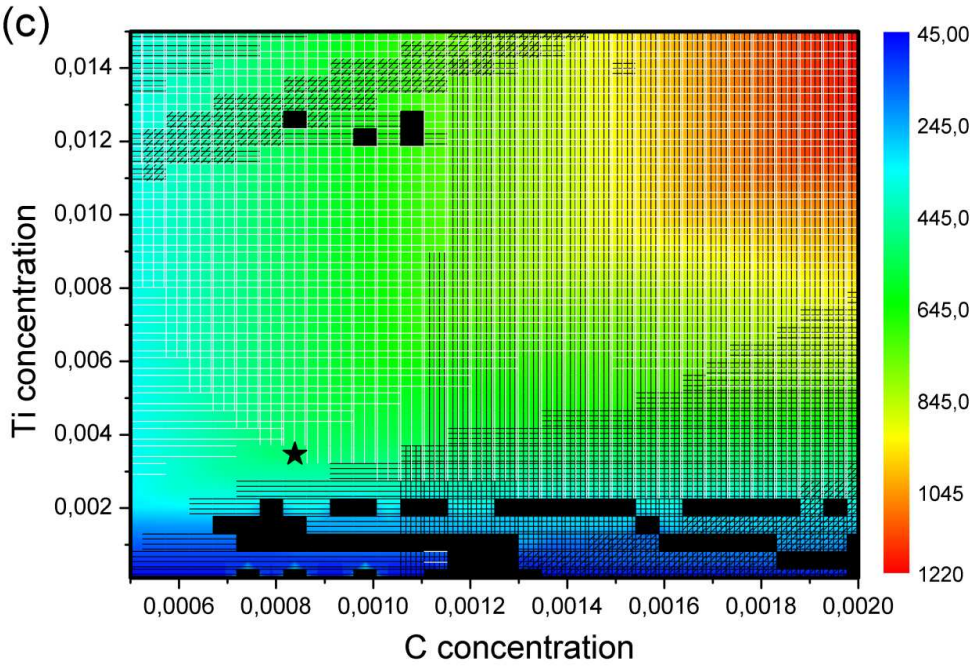

108x74mm (300 x 300 DPI)

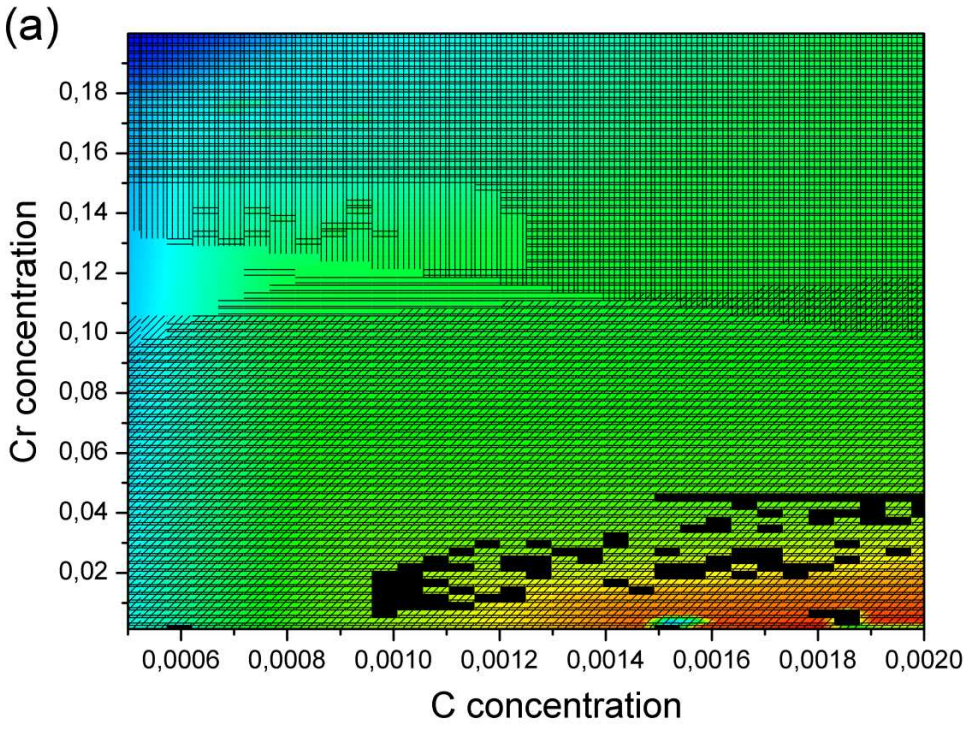

99x74mm (300 x 300 DPI)

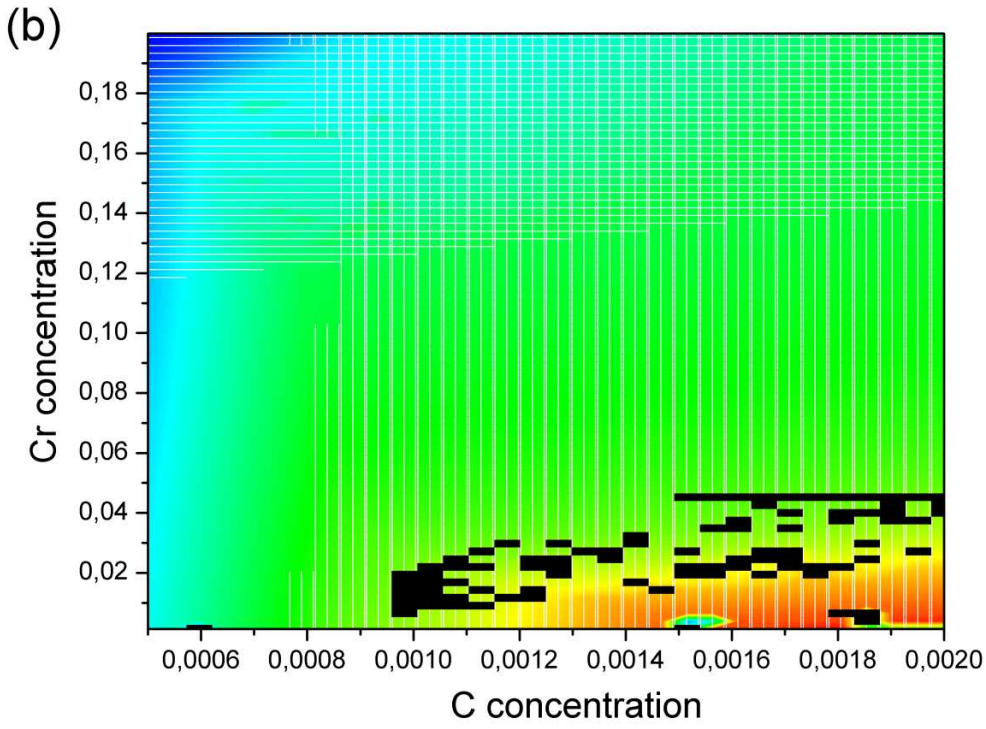

99x74mm (300 x 300 DPI)

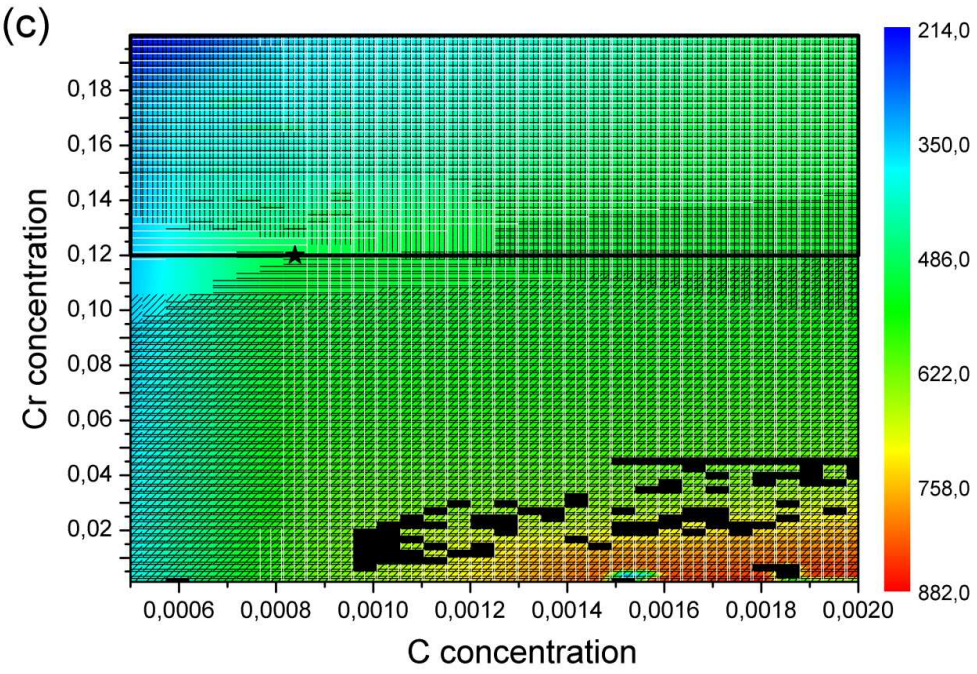

108x74mm (300 x 300 DPI)

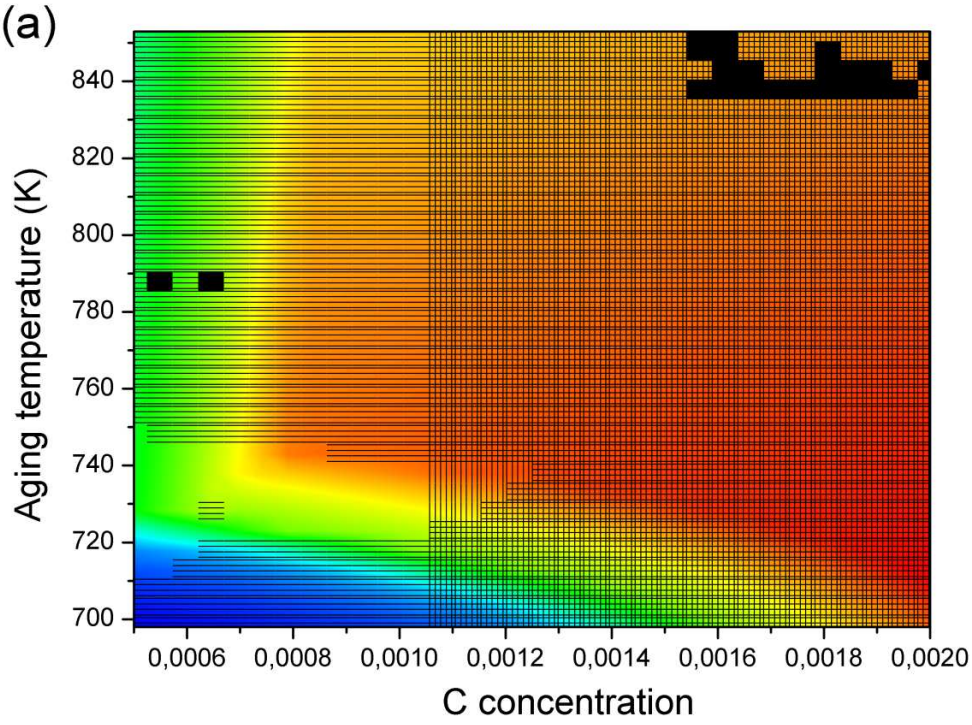

99x74mm (300 x 300 DPI)

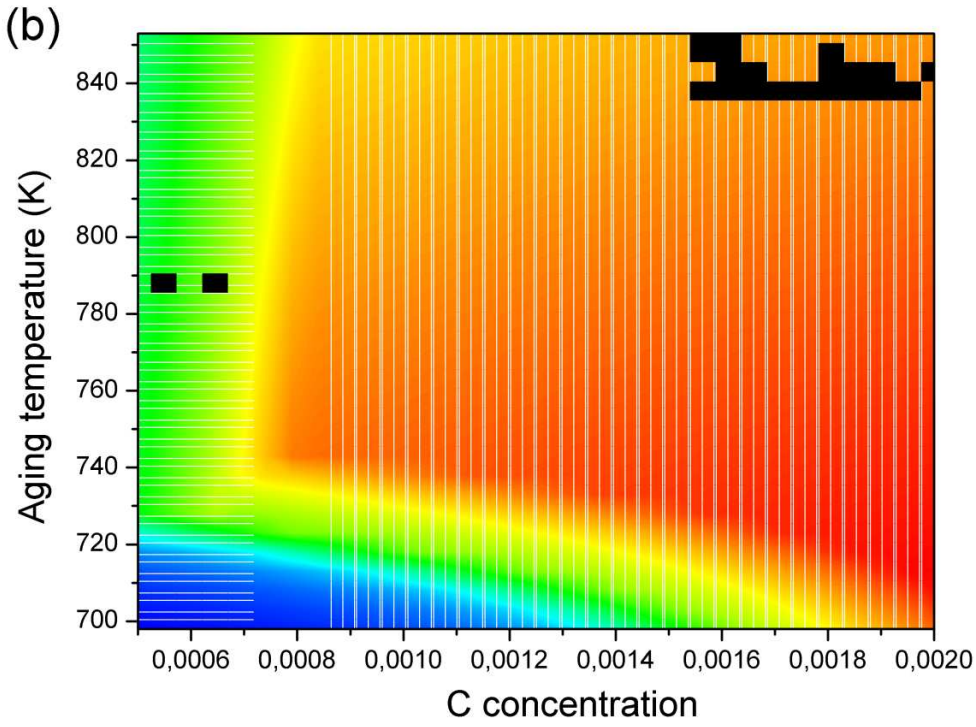

99x74mm (300 x 300 DPI)

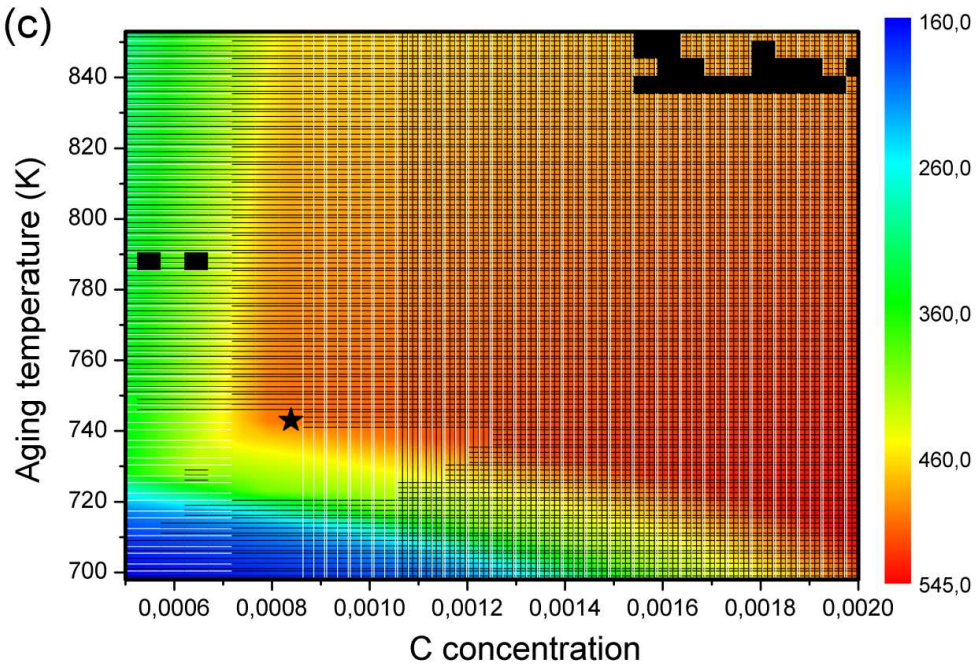

107x74mm (300 x 300 DPI)

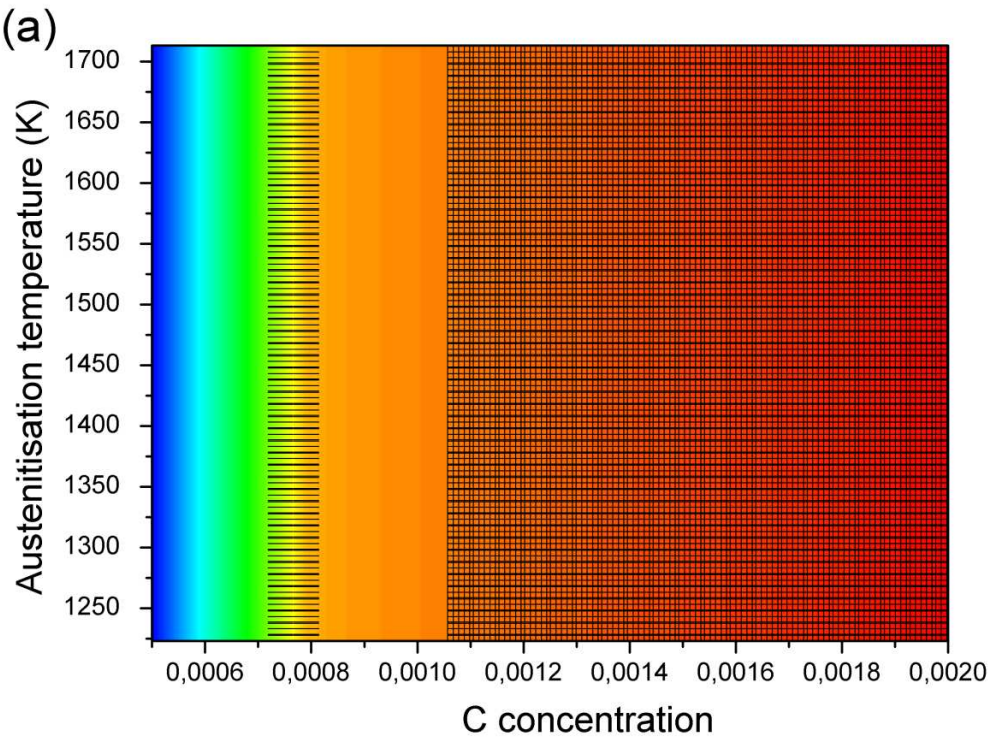

99x74mm (300 x 300 DPI)

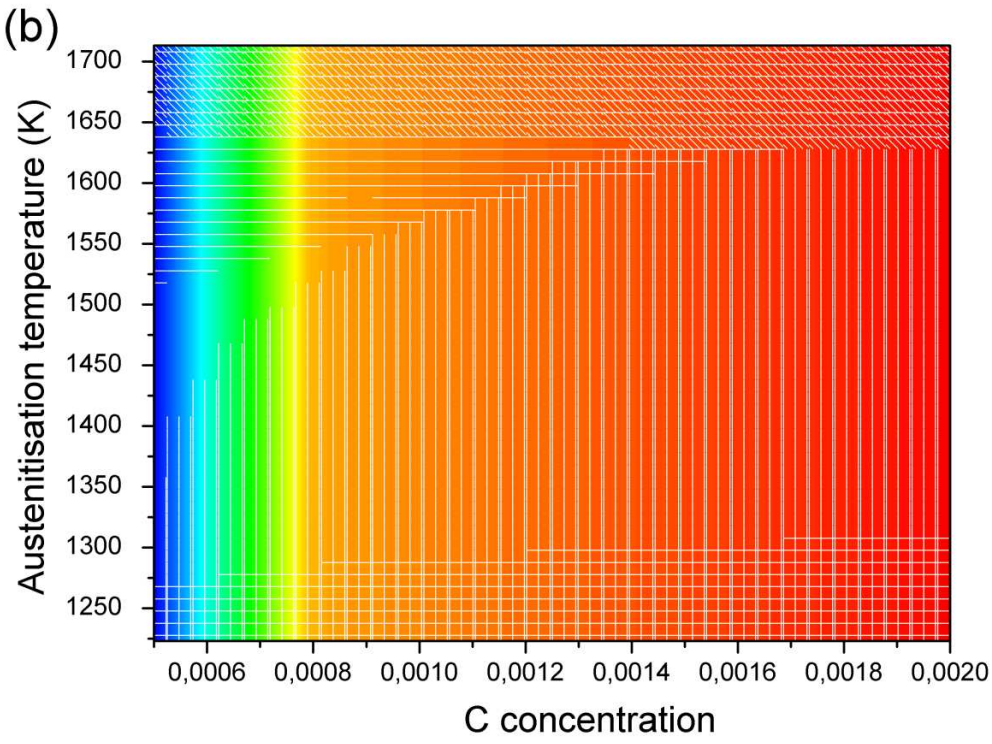

99x74mm (300 x 300 DPI)

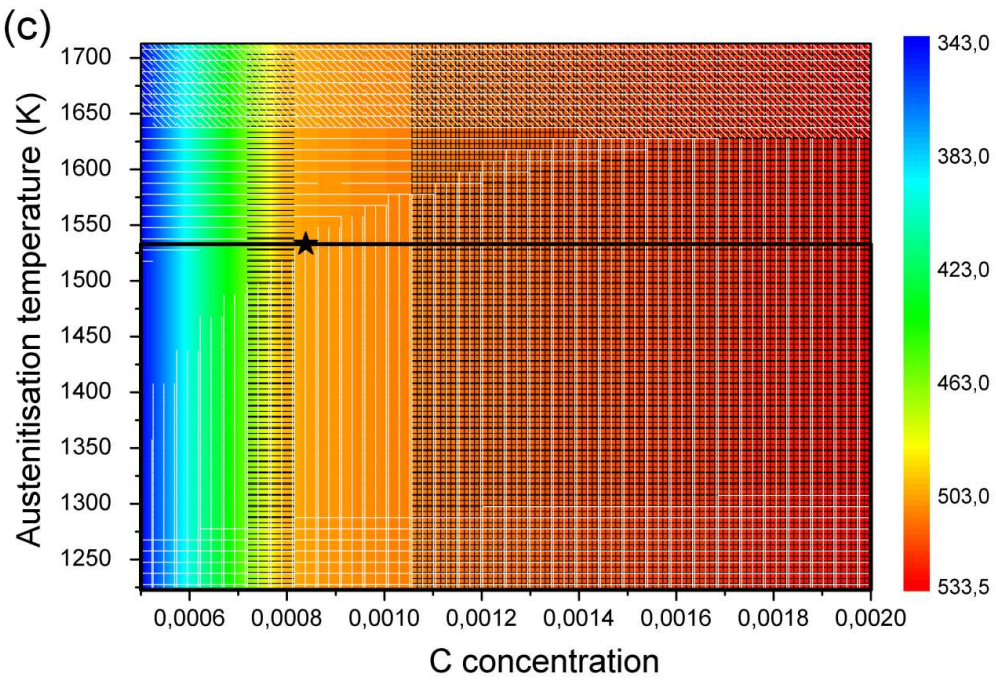

108x74mm (300 x 300 DPI)

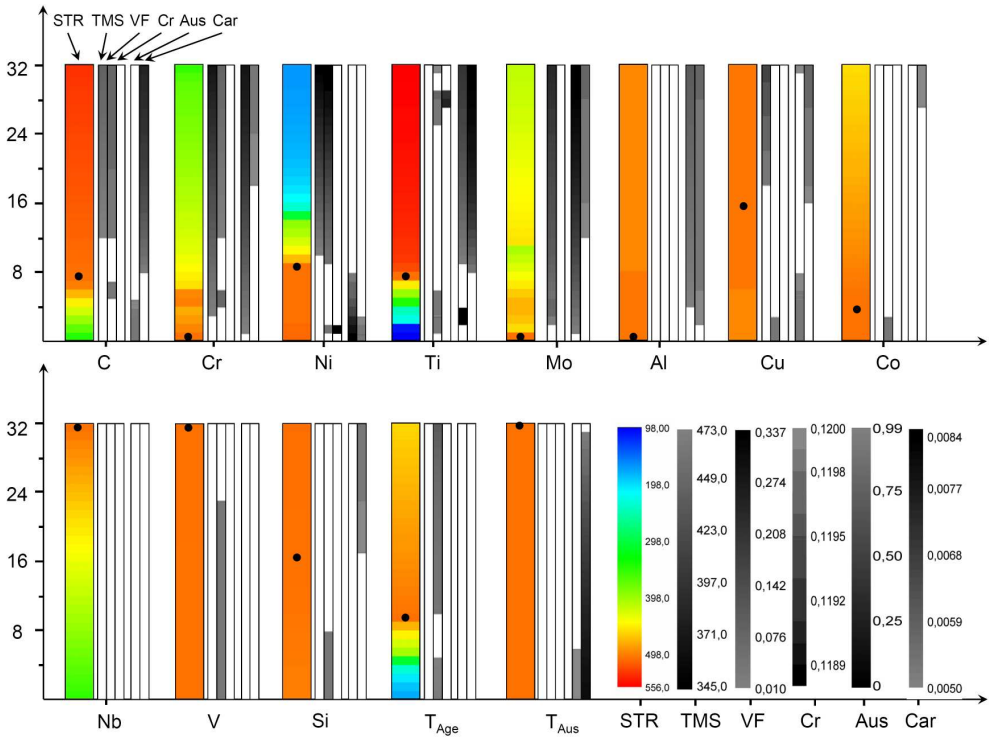

149x111mm (300 x 300 DPI)